Modeling of Industrial Fluidized-Bed Reactors

Joachim Werther* and Ernst-Ulrich Hartge

Department of Chemical Engineering, Technical University Hamburg-Harburg, D 21071 Hamburg, Germany

A modeling approach is presented that is able to handle the most important aspects of industrial fluidized-bed reactors. A particular focus is to describe the relationship between catalyst attrition, solids recovery in the reactor system, and chemical performance of the fluidized-bed reactor. The competing influences of attrition of the catalyst particles and efficiency of the solids recovery lead to the establishment of a catalyst particle size distribution in the bed inventory, which, in turn, influences via the hydrodynamic characteristics of the fluidized bed and, thereby, the performance of the chemical reactor. The usefulness of this approach is illustrated with model calculations for a fictituous first-order reaction in which the fluidized bed is equipped with different solids recovery systems including one single-stage cyclone, several cyclones in parallel, and two- and three-stage cyclone systems. Model calculations illustrate the importance of a high efficiency of solids recovery to keep the fines in the system which is decisive for a high performance of the reactor. The calculations reveal that it might take months until a quasi-steady state of the bed particle size distribution is obtained.

1. Introduction

A sketch of a typical fluidized-bed reactor for catalytic reactions operated in the bubbling-bed mode is shown in Figure 1. The fluidizing gas enters the bed via the gas distributor. Educts can be contained in the fluidizing gas and/or can be separately introduced into the bed. Inside the bubbling bed, the reaction takes place in contact with the catalyst particles, and heat can be added or extracted via in-bed tube bundles. Some of the catalyst becomes entrained and sent into the cyclone where most of it is recovered and sent back into the bed. Such reactors have found widespread application in the chemical industry (e.g., Kunii and Levenspiel[1]).

The fluidized-bed reactor has many advantages: excellent gas−solid contacting; no hot spots, even with highly exothermal reactions; good gas-to-particle and bed-to-wall heat transfer; and ease of solids handling, which is particularly important if the catalyst ages quickly. However, the list of disadvantages of fluidized-bed reactors is equally as long: broad residence time distributions of the gas due to dispersion and gas-bypass in the form of bubbles, broad residence time distributions of solids due to intense mixing, erosion of the bed internals, and attrition of the catalyst particles. A particular disadvantage of the fluidized-bed reactor is its difficult scale-up. The historical experience with the FCC process is that, in the early 1940s, this process was successfully scaled up from a 5-cm-diameter pilot-scale unit to a 4.5-m-diameter bed in a production unit.[1] On the other hand, around 1950, the development of the Fischer−Tropsch synthesis in a fluidized bed that was carried out in the U.S. failed completely: after good results on the bench and pilot scales, the technical plant reached only 1500−2000 barrels/day instead of the planned 7000 barrels/day.[2]

Modern process design should be able to avoid such disasters by making use of modeling and simulation tools. However, a modeling tool that is truly helpful in planning and designing of a *technical* fluidized-bed reactor has to fulfill several requirements. It should be able to describe the influence of the several changes that are typical for the scale-up process, for example, enlargement of bed diameter, bed height, and fluidizing velocity; changes of the gas distributor design; and introduction of in-bed heat exchanger tubes and baffles.

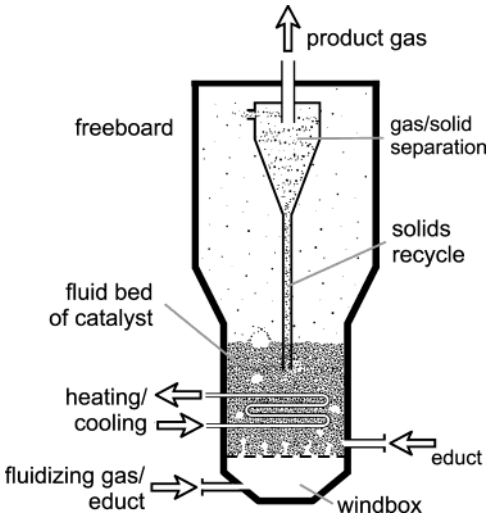

Figure 1. Schematic representation of a fluidized-bed reactor.

Early fluidized-bed reactor models[3−6] were not well-suited for predictive scale-up purposes but rather were intended for the interpretation of measured performance data, as they assumed the mass-transfer area between the bubble and suspension phases to be uniformly distributed over the height of the bed, thus leading to a characteristic height of a transfer unit (HTU) or number of transfer units (NTU). Closer to physical reality were the bubble-based reactor models, the most prominent being the model by Kunii and Levenspiel.[1] More recently, modeling of multiphase flows is often based on first principles, but it should be stated here that computational fluid dynamics (CFD) models (e.g., Gidaspow,[7] Li and Kuipers[8]) are not yet sufficiently developed to be effective tools for the design of technical

* To whom correspondence should be adressed. Tel.: 49-40-42878-3039. Fax: 49-40-42878-3039. E-mail: Werther@tu-harburg.de.

10.1021/ie030760t CCC: $27.50
Published on Web 07/13/2004

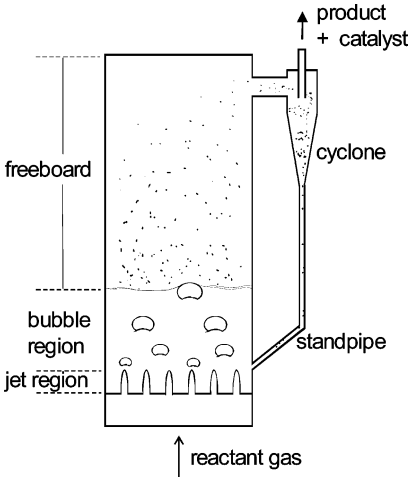

Figure 2. Fluidized-bed reactor model system.

fluidized-bed reactors. The reason for this inadequacy lies first in the complexity of the gas−solid flow in fluidized beds, which makes computations so complicated and time-consuming that the additional consideration of chemical reactions and particularly the handling of the necessarily large geometries of technical reactors easily exceeds the presently available computing capacities.

In the present work, a fluidized-bed reactor model based on the "traditional" bubble model approach is presented that is able to handle the most important aspects of a technical reactor. A particular focus is to describe the relationship between the catalyst attrition and the chemical performance of the fluidized-bed reactor. As a model case, the coupling of a fluidized-bed reactor with a solids recovery device is modeled that leads, under the competing influences of attrition of the catalyst particles and efficiency of the solids recovery, to the establishment of a catalyst particle size distribution (PSD) in the bed inventory. The PSD, in turn, via the hydrodynamic characteristics of the bed, influences the performance of the chemical reactor.

2. Theory

2.1. Particle Population Balance for the Fluidized-Bed System. The system to be modeled is shown in Figure 2. The reactant gas enters the fluidized bed via the distributor. As an example of a technical gas distributor, a multiorifice plate has been chosen. From the orifices, gas jets issue into the bed. At the tips of the jets, bubbles form that might coalesce or split during their rise in the bed. At the surface of the bed, the bubbles erupt, and catalyst particles are thrown into the freeboard. This latter region is characterized by a decay of the solids volume concentration with height. Finally, some catalyst is carried over to the cyclone, where most of the particles are recovered from the exiting gas and sent back to the reactor. According to the cyclone's separation efficiency curve, some fines will leave the cyclone with the product gas. Chemical conversion will occur in both the jet and the bubble regions. Although it might be significant in some cases, chemical reaction in the freeboard region and inside the cyclone is neglected in the present work.

One of the goals of the present work is a description of the catalyst particle size distribution that is established in the fluidized-bed system over the course of time as a consequence of attrition in various parts of the loop

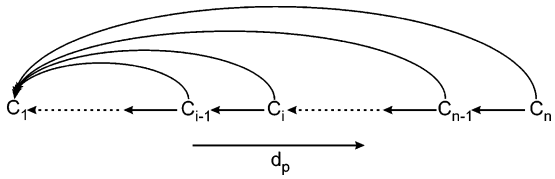

Figure 3. Abrasion-induced mass transfer between particle size intervals.

and as a result of the efficiency of the solids recovery unit. Such a description requires that the fate of the particles in the individual size classes be followed. This is conveniently done on the basis of a particle population balance that describes fines production and particle shrinking due to the individual attrition sources, as well as the particle-size-dependent transport between these regions.

Because catalyst attrition under normal operating conditions usually follows the mode of pure abrasion,[15] it results in the production of fines and the corresponding shrinking of the mother particles, as shown schematically in Figure 3. In the following discussion, this abrasion mode is assumed to be valid throughout the whole system. As a first approximation, the initial breakage of fresh catalyst is neglected here.

Of course, abrasion is a very particular mode of comminution. It will only be the governing mechanism if the fluidized-bed system is operated properly and if the catalyst is designed accordingly. If, for example, because of the improper design of a multihole gas distributor, gas velocities exceed roughly 90 m/s or cyclone velocities during operation exceed about 25 m/s, or if the catalyst is simply too weak, fragmentation will occur, which is a completely different mechanism. This latter mechanism is not considered in the present model because the occurrence of catalyst fragmentation will almost inevitably lead to excessive loss of material and thus cannot be a basis for normal reactor operation.

Focusing on a discretized particle size distribution, the particular effect of abrasion can be illustrated with Figure 3. During the time interval Δt, a mass $m_{\mathrm{att},i}$ of fines is transferred from C_i into the smallest size class C_1, which collects all abrasion-produced fines. It can be assumed that all particles of the size interval C_i are involved in the generation of these fines. As a consequence, all particles are shrinking, and some of them become smaller than the lower bound of their size interval. They must thus be assigned to the smaller size interval C_{i-1}. This mass transferred between neighboring intervals is denoted by $m_{i,i-1}$.

On the other hand, the rest of the material remains in its original size interval, even though the particles are also reduced in size. These mass-transfer phenomena can be summarized in a set of mass balances for the individual size fractions

$$\mathrm{d}m_i = -m_{\mathrm{att},i} - m_{i,i-1} + m_{i+1,i} \qquad i = 2, \ldots, n-1 \quad (1)$$

where n is the number of size intervals. An exception is made for both the interval of the finest particles, C_1, and the interval of the coarsest particles, C_n. The interval C_1 receives all abrasion-produced fines originating from the other size intervals, as well as the shrunken particles from the neighboring size interval, C_2. However, there is no material loss from C_1 due to a further attrition of the particles within this interval. Even if there were further particle degradation, the attrition products would still remain within the size

interval C_1. On the other hand, the particles within the size interval C_n undergo abrasion. This results in both the loss of fine material and the loss of shrunken particles. However, there is no coarser size fraction from which interval C_n could receive shrunken particles.

$$\mathrm{d}m_1 = \sum_{i=2}^{n} m_{\mathrm{att},i} + m_{2,1} \tag{2}$$

$$\mathrm{d}m_n = -m_{\mathrm{att},n} - m_{n,n-1} \tag{3}$$

To apply the set of mass balances of eqs 1−3, both the fines production, $m_{\mathrm{att},i}$, and the mass transfer to the neighboring size interval, $m_{i,i-1}$, must be known for each size interval.

The mass loss due to attrition, $m_{\mathrm{att},i,\mathrm{p}}$, for a single particle in size class i is related to the mass loss, $m_{\mathrm{att},i}$, of all particles in this interval by

$$m_{\mathrm{att},i,\mathrm{p}} = \frac{m_{\mathrm{att},i}}{N_{\mathrm{p},i}} \tag{4}$$

where $N_{\mathrm{p},i}$ denotes the number of particles in size class i. This latter number can be calculated from the total mass, m_{tot}, of all particles and the mass fraction, $\Delta Q_{3,i}$, of size class i in the particle size distribution if spherical particles with the diameter d_{p} are assumed

$$N_{\mathrm{p},i} = \frac{6 m_{\mathrm{tot}} \Delta Q_{3,i}}{\pi {d_{\mathrm{p},i}}^3 \rho_{\mathrm{s}}} \tag{5}$$

where ρ_s is the catalyst's apparent density.

It follows that

$$m_{\mathrm{att},i,\mathrm{p}} = m_{\mathrm{att},i} \frac{\pi {d_{\mathrm{p},i}}^3 \rho_{\mathrm{s}}}{6 m_{\mathrm{tot}} \Delta Q_{3,i}} \tag{6}$$

At the end of the time interval Δt, i.e., at the time $t + \Delta t$, the mass of a single particle of mean size in i is

$$m_{i,\mathrm{p},t+\Delta t} = m_{i,\mathrm{p},t} - m_{\mathrm{att},i,\mathrm{p}} \tag{7}$$

Assuming an unchanged spherical shape, it follows that

$$d_{\mathrm{p},i,t+\Delta t} = \sqrt[3]{\frac{6}{\pi}\left(\frac{\pi}{6} {d_{\mathrm{p},i,t}}^3 - \frac{m_{\mathrm{att},i,\mathrm{p}}}{\rho_{\mathrm{s}}}\right)} \tag{8}$$

Inserting eq 6 into eq 8 finally yields the following expression for the change in diameter of a particular particle in i

$$\Delta d_{\mathrm{p},i} = d_{\mathrm{p},i,t} - d_{\mathrm{p},i,t+\Delta t} = d_{\mathrm{p},i,t}\left(1 - \sqrt[3]{1 - \frac{m_{\mathrm{att},i}}{m_{\mathrm{tot}} \Delta Q_{3,i}}}\right) \tag{9}$$

Shrinking of all particles in i by $\Delta d_{\mathrm{p},i}$ means that a certain mass from this size class will travel into size class $i - 1$. This traveling mass is denoted by $m_{i,i-1}$ and can be calculated from the relationship

$$\frac{m_{i,i-1}}{(m_i - m_{\mathrm{att},i})} = \frac{\Delta d_{\mathrm{p},i}}{d_{\mathrm{p},i+1} - d_{\mathrm{p},i}} \tag{10}$$

which is obvious from the graphical representation in Figure 4.

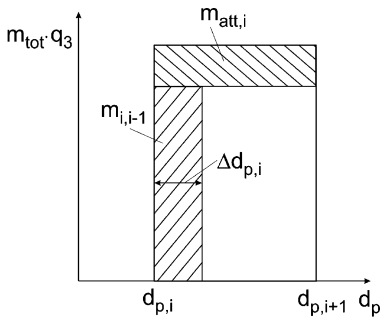

Figure 4. Mass loss from in size class i due to abraded fines ($m_{\mathrm{att},i}$) and shrinking of mother particles ($m_{i,i-1}$).

2.2. Fluid Dynamics of the Bubbling Fluidized Bed. The fluidized bed is assumed to be equipped with a multihole distributor that has n_{or} orifices and a total cross-sectional area of A_{t}. With the superficial fluidizing velocity u, we obtain the volumetric flow, $\dot{V}_{\mathrm{or}}$, through a single opening as

$$\dot{V}_{\mathrm{or}} = \frac{u A_{\mathrm{t}}}{n_{\mathrm{or}}} \tag{11}$$

which, according to Davidson and Harrison,[16] will lead to the formation of bubbles with an initial diameter of the volume-equivalent sphere

$$d_{\mathrm{v},0} = 1.3\left(\frac{{\dot{V}_0}^2}{g}\right)^{0.2} \tag{12}$$

Because we are considering a multihole distributor, these bubbles are formed at the tip of the jets issuing from the individual holes. The jet length L can be estimated, for example, from the correlation suggested by Merry.[11]

On the basis of the pioneering work by Clift and Grace[12,13] on the mechanism of bubble coalescence in gas-fluidized beds, one of the present authors (Werther[14]) developed a model for bubble growth in freely bubbling fluidized beds that was later extended to the consideration of the combined action of coalescence and splitting of the bubbles by Hilligardt and Werther.[15] According to the latter work, the growth of the bubble volume-equivalent sphere diameter d_{v} with height h for a catalyst that belongs to the Geldart A group of powders is given by

$$\frac{\mathrm{d}(d_{\mathrm{v}})}{\mathrm{d}h} = \left(\frac{2\epsilon_{\mathrm{b}}}{9\pi}\right)^{1/3} - \frac{d_{\mathrm{v}}}{3\lambda u_{\mathrm{b}}} \tag{13}$$

where the first term describes growth by coalescence and the second term accounts for bubble splitting. λ is the mean duration of life of a bubble with diameter d_{v}, which can be calculated from the relation[15]

$$\lambda = 280\frac{u_{\mathrm{mf}}}{g} \tag{14}$$

The local bubble volume fraction, ϵ_{b}, is given by

$$\epsilon_{\mathrm{b}} = \frac{\dot{V}_{\mathrm{b}}}{u_{\mathrm{b}}} \tag{15}$$

where the visible bubble flow, $\dot{V}_b$, can be approximated for a Geldart A powder by

$$\dot{V}_b \approx 0.8(u - u_{mf}) \tag{16}$$

The local bubble rise velocity u_b is given by[18]

$$u_b = \dot{V}_b + 0.71\vartheta\sqrt{g d_v} \tag{17}$$

with

$$\vartheta = \begin{cases} 1.18 & \text{for } d_t < 0.05 \text{ m} \\ 3.2 d_t^{0.33} & \text{for } 0.05 \text{ m} \le d_t \le 1 \text{ m} \\ 3.2 & \text{for } d_t > 1 \text{ m} \end{cases} \tag{18}$$

where d_t denotes the bed diameter.

The mass of solids in the freeboard is neglected for these calculations, i.e., the total mass in the reactor, m, is assumed to be concentrated inside the bed. Thus, the total mass can be calculated from

$$m = A_t \rho_s \left(\int_0^{H_j} c_v \, dh + \int_{H_j}^{H_b} c_v \, dh\right) \tag{19}$$

With regard to the attrition in the cyclone, it is necessary to know the entrainment flux, $G_{s,\infty}$, above the transport disengaging height (TDH) (if we assume an adequately designed, sufficiently high vessel). This entrainment flux can be calculated from the work of Geldart and Tasirin,[16] who investigated the entrainment of FCC-type catalysts from bubbling fluidized beds

$$G_{s,\infty} = \sum_{i=1}^{n} G_{s,i,\infty} \tag{20}$$

where

$$G_{s,i,\infty} = K_i^* x_i \tag{21}$$

x_i is the mass fraction within the ith size interval (mean particle size $d_{p,i}$) of the bed inventory. The parameter K_i^* denotes the elutriation rate constant for an individual particle size class i and is calculated from

$$K_i^* = 14.5 \rho_f u^{2.5} \exp\left(-5.4 \frac{u_{t,i}}{u}\right) \text{[kg/(m}^2\text{·s)]} \tag{22}$$

In this latter correlation, $u_{t,i}$ is the terminal velocity of a particle with size $d_{p,i}$ under the operating conditions of the fluidized bed.

2.3. Catalyst Attrition in the Fluidized Bed. Catalyst attrition in the fluidized bed is assumed to be restricted to the jetting region and to the bulk of the bubbling bed. Attrition in the freeboard is, as a first approximation, simply neglected. From jet attrition in the n_{or} jets, we obtain a mass production of fines resulting from the size fraction i of[17]

$$\dot{m}_{att,jet,i} = n_{or} c_j d_{p,i} \rho_f {d_{or}}^2 {u_{or}}^3 \tag{23}$$

Attrition due to bubbles is given by[18,19]

$$\dot{m}_{att,bubble,i} = c_b d_{pi} m_b (u - u_{mf})^3 \tag{24}$$

where the mass in the bubbling bed region, m_b, can be taken from eq 19.

2.4. Chemical Conversion in the Fluidized Bed. To model the chemical conversion in the bubbling fluidized bed, the following simplifying assumptions are made:

(i) The fluidized bed is divided into two phases. One phase is the disperse solid-free phase that includes the bubbles and grid jets. The other phase is the continuous suspension phase that surrounds the jets and bubbles.

(ii) The volume of the fluidized bed is separated into the jetting region close to the distributor, the height (H_j) of which is given by the penetration depth of the jets, and the bubbling region, which occupies the rest of the bed.

(iii) We consider here beds of catalyst that belong to the Geldart group A of powders. For such powders, under technical operating conditions, the superficial velocity u in the fluidized bed will always be much greater than the minimum fluidizing velocity u_{mf}. As a consequence, the throughflow velocity in the suspension phase is described with sufficient accuracy by u_{mf}/ϵ_{mf}, where ϵ_{mf} is the bed porosity under minimum fluidization conditions.

(iv) We assume plug flow of gas in both phases.

(v) Both bubbles and grid jets are assumed to be solids-free, i.e., the heterogeneously catalyzed gas-phase reaction occurs in the suspension phase only.

(vi) Mass transfer between the bubble and suspension phases is described by a correlation suggested by Sit and Grace[20]

$$k_G = \frac{u_{mf}}{3} + \sqrt{\frac{4 D \epsilon_{mf} u_b}{\pi d_v}} \tag{25}$$

where k_G is a height-dependent mass-transfer coefficient that is based on unit reactor volume. d_v und u_b are the local mean bubble size and rise velocity, respectively.

(vii) As a first approximation, the mass-transfer coefficient for the bubble size that is formed at the tips of the jets at a height of $h = H_j$ is assumed to hold for mass transfer across the surface of the grid jets as well.

(viii) The geometry of a single grid jet is simplified to a truncated cone. The half-angle α of the opening of the cone is assumed to be 7.5° following the results by Basov et al.[21] and Merry.[11]

(ix) No change in volumetric gas flow due to reaction is considered (this effect has been taken into account, e.g., by Sitzmann et al.[22]).

(x) Possible sorption effects are neglected.

(xi) The catalyst does not age.

Following these assumptions, for the case of a simple first-order heterogeneously catalyzed reaction, the mass balances on a reactor volume element $A_t \, dh$ in the bubble and suspension phases are, respectively, given by

$$\epsilon_b \frac{\partial C_b}{\partial t} = -[u - u_{mf}(1 - \epsilon_b)] \frac{\partial C_b}{\partial h} - k_G a (C_b - C_d) \tag{26}$$

$$(1 - \epsilon_b)[\epsilon_{mf} + (1 - \epsilon_{mf})\epsilon_p] \frac{\partial C_d}{\partial t} = -u_{mf}(1 - \epsilon_b) \frac{\partial C_d}{\partial h} + k_G a (C_b - C_d) + (1 - \epsilon_b)(1 - \epsilon_{mf}) k_m \rho_s C_d \tag{27}$$

where C_b and C_d are the reactant concentrations in the solid-free and suspension phases, respectively. k_m is the

reaction rate constant of the first-order chemical reaction. At the distributor level, it holds that

$$C_b = C_d = C_0 \qquad h = 0 \tag{28}$$

where C_0 denotes the reactant concentration in the feed gas.

A decisive parameter is the specific mass-transfer area a between the two phases. In the bubbling region, a is given by

$$a = \frac{6\epsilon_b}{d_v} \qquad H_j \le h \le H_b \tag{29}$$

In the jetting region, the local specific mass-transfer area is given by

$$a = \frac{n_{or}}{A_t}\frac{2\pi}{\cos\alpha}\left(\frac{d_{or}}{2} + h\tan\alpha\right) \qquad 0 < h < H_j \tag{30}$$

2.4. Fluid Dynamics and Attrition in the Cyclone. In the present model, the cyclone is relevant for two mechanisms. First, the incoming solids are separated according to the cyclone's fractional separation curve. In addition to this separation, however, the particles entering the cyclone are subjected to attrition. These two mechanisms are modeled in series, with the attrition being the first mechanism and the separation being the second. This means that the already-attritted material is subjected to the separation process. A possible reaction in the cyclone is neglected.

The sequence of modeling attrition first and then separation is a consequence of an experimental observation:[25] the internal wall of a cyclone was painted, and the erosion marks were examined after some time of operation. Severe erosion marks were observed on the wall just at the transition from the entry duct to the cylindrical cyclone wall, which led the authors to believe that it is the region inside the cyclone where most of the attrition occurs and which justifies the sequence of calculation beginning with attrition and followed by separation of the solids.

The separation in the cyclone is described according to the design rules given in the VDI Heat Atlas.[23] Because the solids loading is distinctly higher than its critical value in typical fluidized-bed processes, the gas–solids separation is described according to the "critical load hypothesis" suggested by, e.g., Trefz and Muschelknautz,[24] which divides the cyclone separation into the sequence of a spontaneous separation of the surplus mass at the cyclone inlet and a subsequent so-called "inner separation" of the remaining critical mass inside the vortex. The standard German design procedure[26] assumes an empirically found size distribution of the particles that are subjected to separation in the vortex. This procedure cannot, however, be used in connection with population balancing. In the present work, it is therefore assumed that the spontaneous separation at the cyclone inlet is nonclassifying. Therfore, the remaining critical mass that is subjected to separation in the vortex has the same particle size distribution as the solids that are entering the cyclone.

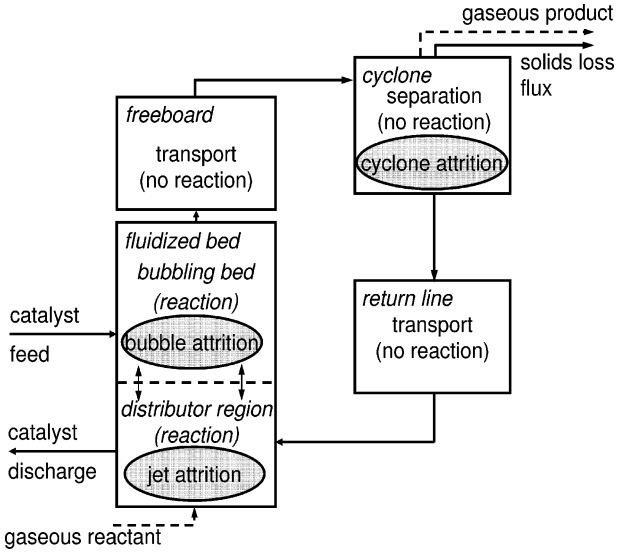

Figure 5. Modeling steps in a fluidized-bed reactor system.

According to Reppenhagen and Werther,[25] attrition in the cyclone is described by

$$\dot{m}_{att,c,i} = \dot{m}_{c,in,i} c_c d_{p,c,i} \frac{u_{c,in}^2}{\sqrt{\mu_c}} \tag{31}$$

Here, $\dot{m}_{att,c,i}$ is the mass flow of fines produced by attrition when a solids mass flow $\dot{m}_{c,in,i}$ of solids in the ith size interval with a mean particle size of $d_{p,c,i}$ enters the cyclone. μ_c is the solids loading of the incoming gas flow

$$\mu_c = \frac{\dot{m}_{c,in}}{A_t u \rho_g} \tag{32}$$

where u is the superficial velocity in the reactor. $u_{c,in}$ is the gas velocity in the cyclone inlet. The total inflowing solids mass flow is

$$\dot{m}_{c,in} = \sum_{i=1}^{n} \dot{m}_{c,in,i} \tag{33}$$

2.5. Calculation of the Solids Loop. The model layout is given in Figure 5. It consists of separate modules for the three components fludized bed, cyclone, and standpipe. These components are connected by the streams of solids flowing from one module to another. The boundaries of the modules are chosen such that all of the couplings between the modules are always only in one direction. This allows the modules to be computed independently in a sequence. The simulation is nonstationary and allows the development of the particle sizes to be followed as a function of time.

For the standpipe, plug flow of the solids is assumed, and attrition in the standpipe is neglected. Therefore, the standpipe will influence only the dynamics of the system; the steady-state results do not depend on the design of the standpipe at all.

The calculation of the solids loop is schematically shown in Figure 6. The computation starts with given masses of fresh catalyst in the fluidized bed and the standpipe. No solids hold-up in the cyclone is assumed. The calculation is then done in the sequence fluidized bed, cyclone, and standpipe. Then, the whole loop is

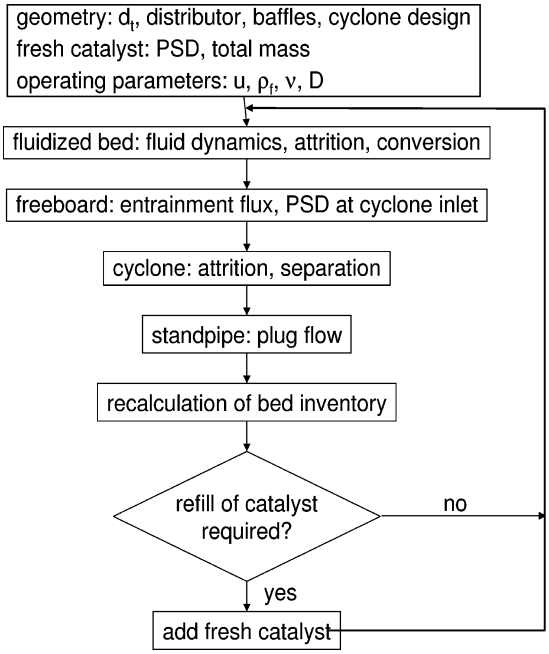

Figure 6. Calculation of the solids loop.

repeated. The calculation is done with time steps Δt between 0.5 and 20 s. The time step always has to be chosen such that the mass leaving a certain particle size class is always significantly less than the mass in this size class. This condition must be valid for all classes and for all modules. The mass of catalyst in the reactor adjusts itself such that the total mass balance is fulfilled.

The loss of solids has to be compensated by the addition of fresh catalyst. In the present model, this feeding of fresh catalyst is done discontinuously. Whenever the solids hold-up in the reactor falls below a certain value, given as a percentage of the inventory at the beginning, fresh catalyst is fed to the reactor. This feeding is completed within one time step. The layout of the model also allows for the replacement of aged catalyst by fresh catalyst, but for the calculations presented in the following section, this replacement has not been simulated.

Chemical reactions are assumed to take place only in the fluidized bed. Reactions in the freeboard, the cyclone, and the standpipe are neglected in the present work.

3. Results and Discussion

It would have been nice to validate the model as a whole against performance data of a large-scale industrial fluidized-bed reactor. However, if such detailed data exist at all, they will always be proprietary. Therefore, the authors can only argue that the individual elements of the model have all been validated in separate investigations as follows:

(i) The bubble coalescence and splitting model (eq 13), which contains the influence of the bed particle size, was validated by Hilligardt and Werther[15] with bubble size measurements in catalyst fluidized beds.

(ii) The influence of fluid mechanics on the chemical conversion (eqs 26 and 27) was investigated by Bauer et al.[32] They compared model predictions with measurements of ozone conversion in catalyst beds with diameters between 0.2 and 1 m equipped with different gas distributor designs. Bauer and Werther[30] and Werther[33] compared model predictions with reactor performance data taken from the patent literature.

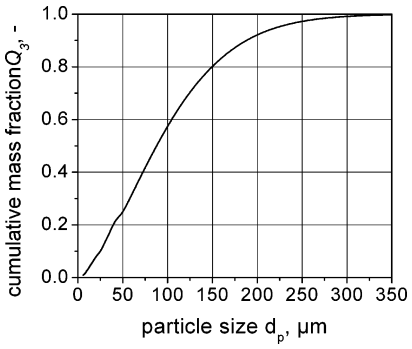

Figure 7. Particle size distribution of the fresh catalyst.

(iii) The attrition models were validated by experiments by Werther and Xi[17] for grid jet attrition, by Xi[18] and Werther and Reppenhagen[19] for bubble-induced attrition, and by Reppenhagen and Werther[25] for attrition in the cyclone.

(iv) The effect of attrition on the development of the particle size distribution was modeled and validated with measurements by Reppenhagen and Werther.[26]

(v) The model for the solids recovery in the cyclone that is found in the VDI Heat Atlas[23] has been validated many times in industrial applications.

Thus, the individual elements have been thoroughly validated, and this should lend some confidence to the overall model presented here.

3.1. Definition of the Test System. The purpose of the present work is to study the interrelation of attrition and solids separation in a fluidized-bed system and its effect on the chemical conversion. Because we are not aiming at a specific application, the data for the test system were more or less arbitrarily chosen, although the choice was made on the basis of the authors' consulting experience. The following data are assumed:

For the first-order catalytic reaction under consideration, it holds that, under process conditions (1 bar, 723 K), $k_m = 0.0067$ m^3/(kg·s). The gas is assumed to have the same viscosity and density as air under these conditions. The numerial value of the diffusion coefficient D is 10^{-5} m^2/s.

The catalyst is of the FCC type and belongs to the Geldart group A. Its properties—particle density and attrition characteristics—were taken from previous investigations of the authors' group[26] with samples of industrial catalysts. The PSD of the fresh catalyst is shown in Figure 7. Its Sauter diameter is 46 μm, with 10 mass % below 25 μm, 50 mass % below 87 μm, and 90 mass % below 188 μm. The fraction of fines below 44 μm is 23 mass %. The parameters of the attrition characteristics were experimentally determined as

$$c_j = 9.5 \times 10^{-6}\ \text{s}^2/\text{m}^3$$

$$c_b = 0.4 \times 10^{-3}\ \text{s}^2/\text{m}^4$$

$$c_c = 1.2 \times 10^{-3}\ \text{s}^2/\text{m}^3$$

The voidage of the catalyst bed at minimum fluidization conditions, ϵ_{mf}, is 0.5, and the minimum fluidization velocity, u_{mf}, is 0.0021 m/s. The apparent density, ρ_s, of the catalyst particles is 1500 kg/m^3.

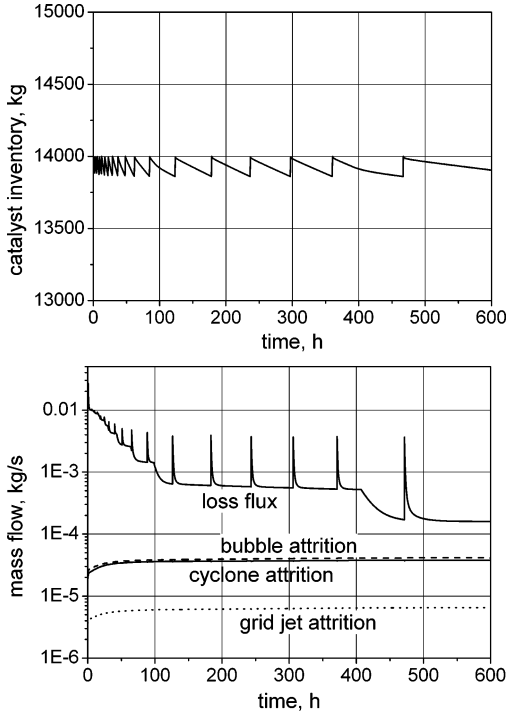

Figure 8. Test case A: one single cyclone for solids recovery.

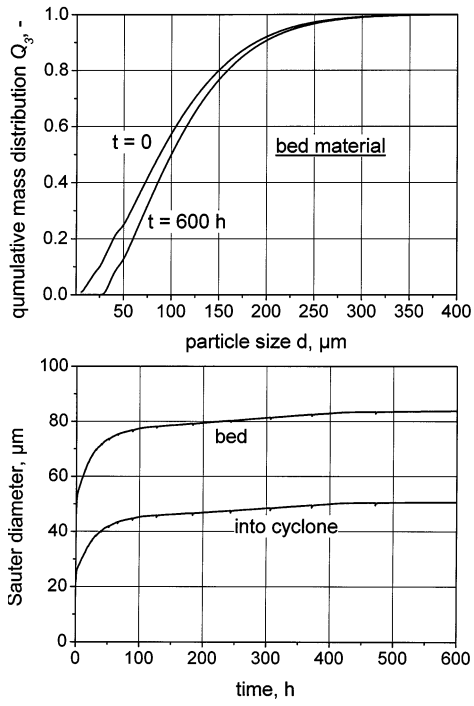

Figure 9. PSD of the bed material before and after 600 h of operation and development of Sauter diameters in the bed and at the cyclone entry with time (test case A).

The cylindrical fluidized-bed vessel has a diameter of 3.5 m. The superficial fluidizing velocity, u, under operating conditions is 0.45 m/s. The catalyst inventory in the system is 14 000 kg. The distributor is of the multihole type with 400 openings per square meter of bed area. The hole diameter is 5 mm, which leads to an orifice velocity of 55 m/s.

In the following calculations of continuous reactor operation, the catalyst loss due to elutriation and attrition is always replaced by adding fresh makeup catalyst when the riser drop deviates by more than 1% from the original value.

The system is equipped with a single cyclone for the first calculations. The cyclone was designed according to the design rules given in the VDI Heat Atlas.[23] As a result, the cyclone has a diameter of 1.5 m, a diameter of the vortex finder tube of 0.5 m, and a total height of 2.5 m.

In the following subsections, different test cases are simulated, starting with the most simple solids recovery by one single-stage cyclone. In further test cases, the solids recovery is varied, i.e., several cyclones in parallel and two- and three-stage cyclone systems are investigated. For each test case, the development of the particle size distribution of the bed inventory is calculated as a function of the operating time, and the effect of the changing particle size distribution on the fluidization characteristics and hence on the chemical performance is assessed. Because bed internals are often used in industrial practice to improve the fluidization behavior, the effect of in-bed screens is also examined.

3.2. Test Case A: Solids Recovery by One Single Cyclone. The cyclone was designed according to ref 23 for a pressure drop of 1600 Pa and an inlet velocity, $u_{c,in}$, of 17.5 m/s. The simulation results show (Figure 8) that, in the start-up phase, obviously, a great deal of fine catalyst is lost through the cyclone. With increasing time of operation, the intervals between the addition of fresh catalyst increase. However, it takes quite a long time before a quasi-steady state is reached. The simulation is now able to explain what happens in detail. The loss flux is the mass flow of solids leaving the system via the cyclone overflow. We see from the spikes in the loss flux vs time that each time immediately after the fresh makeup catalyst has been added, the fines in the fresh catalyst are quickly elutriated. Because the solids are repeatedly recirculated over the cyclone, the system is steadily losing the fine particles. With decreasing fines content in the PSD, the elutriation mass flux from the bed decreases, and the efficiency of separation increases. Both effects explain the decrease of the loss flux with operating time.

The decrease of the loss flux after 400 h is a numerical effect that is due to the discretization of the particle size distribution into 32 classes. By closely examining Figure 8, the reader will be able to observe similar effects (but weaker) at 70 and 100 h as well.

The fines that are lost from the system originate only partly from the fresh catalyst. More significant is the production of fines by attrition. As is shown in Figure 8, in the present case, for given operating conditions, grid and cyclone designs, and solids properties, the contribution of the grid jet attrition is about 1 order of magnitude below the contributions of bubble and cyclone attrition. This is mainly due to the choice of distributor design. Four hundred holes per square meter and a hole diameter of 5 mm lead to an orifice velocity, u_{or}, of about 55 m/s, which is just high enough to create an adequate pressure drop but is low enough to avoid excessive attrition. Note that, according to eq 23, the grid jet attrition is proportional to u_{or}^3. The increase of all attrition fluxes with time is indicative of the increasing mean particle size with time (cf eqs 23, 24, and 31).

Figure 9 compares in its upper part the bed PSD after 600 h with the fresh catalyst's PSD. We see that the content of fines below 44 μm, which is generally considered to be indicative of the fluidization characteristics of a given powder,[27−29] has decreased from over 20% to about 10%. The changing fines content is

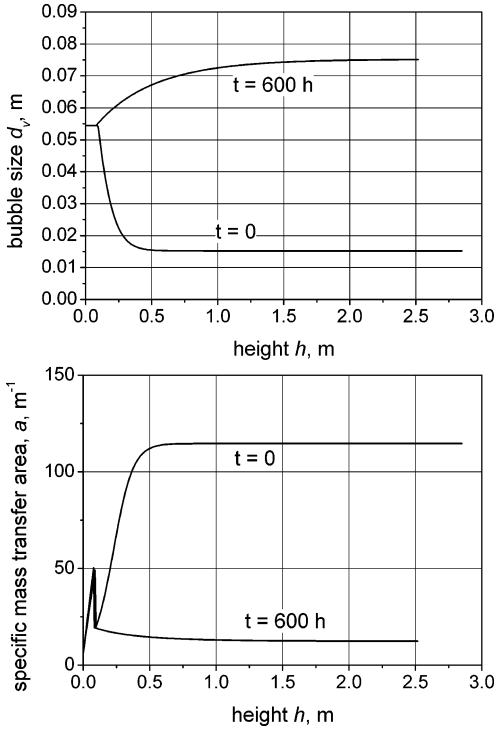

Figure 10. Bubble sizes and mass-transfer areas before and after 600 h of operation (test case A).

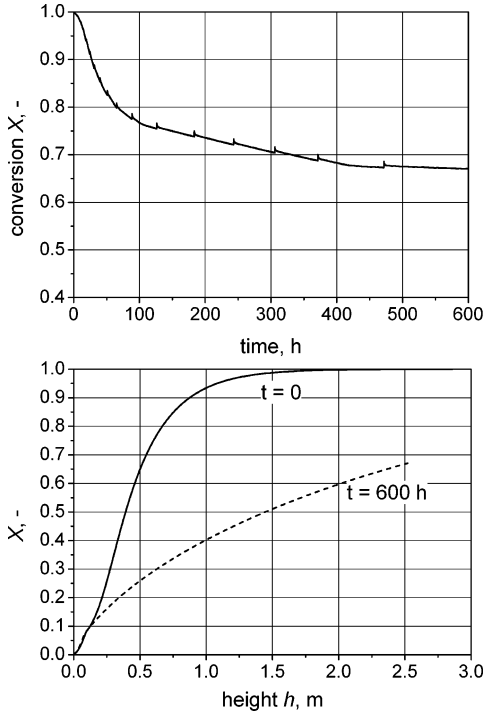

Figure 11. Chemical conversion vs operating time and axial conversion profiles before and after 600 h of operation (test case A).

reflected in the development of the Sauter diameter with time, which is also depicted in Figure 9. The Sauter diameter of the bed material influences the attrition at the grid jets as well as that due to the bubbles, whereas the Sauter diameter at the cyclone inlet is decisive for the extent of attrition in the cyclone.

The change of the Sauter diameter has important consequences, first for the fluid mechanics but then also for the performance of the fluidized bed as a chemical reactor. With increasing Sauter diameter, the minimum fluidization velocity, u_{mf}, increases. Following eq 14, the contribution of the bubble-splitting term in the bubble growth equation (eq 13) is reduced, which means that bubbles grow to larger sizes. This is illustrated in Figure 10. The bubbles that start at the distributor with diameters of around 5.5 cm shrink in size with the original catalyst and reach an equilibrium between coalescence and splitting at a mean diameter of 1.5 cm. On the other hand, after 600 h, the catalyst is largely depleted of fines, which leads to a higher value of u_{mf} and thus less splitting. The resulting equilibrium bubble diameter of 7.5 cm is associated with a dramatically reduced specific mass-transfer area a. Compared to the fresh catalyst at 115 m^2/m^3, the specific mass-transfer area is reduced to about 20 m^3/m^3, which will have consequences for the chemical performance.These consequences are illustrated in Figure 11. We see that the conversion steadily decreases with increasing time of operation of the reactor.

The lower part of Figure 11 illustrates the reactor behavior with both fresh catalyst and after 600 h of operation. With fresh catalyst, the bubbles remain small, and the bed expands to 2.9 m. Because of the large interfacial area of the bubbles, the conversion is practically completed after 2 m in the bed. After 600 h, however, with the coarser bed material and the larger bubbles, the bed expands to only 2.5 m. The smaller interfacial area between the bubbles and the suspension phase reduces the mass transfer, which limits the conversion to about 68%.

3.3. Test Case B: Solids Recovery by One Single Cyclone; Bed with Internals. Internals are frequently used in industry to limit the growth of bubbles or to destroy bubbles in order to increase the specific interfacial area and thereby increase the mass transfer. The conditions of test case A were used again, and screens with mesh widths of 3 cm were inserted at 1 and 2 m above the distributor. Figure 12 shows that the screens reduce the mean bubble size in the bed from about 7 cm to about 5 cm and that this increases the conversion in the reactor from 68% to over 80%. The same effect was observed by the Mitsubishi company in their development of a fluid-bed process for the production of maleic anhydride from the C_4 fraction of the naphtha cracker and was subsequently modeled by Bauer and Werther.[30]

3.4. Text Case C: Solids Recovery by One High-Efficiency Cyclone. A disadvantage of internals is their propensity for erosion. Therefore, a better way to increase the mass transfer in the bed is always to increase the fines content in the bed PSD, which causes the bubbles to split and thereby reduces the equilibrium bubble size. An increase of the fines content should be achievable with a better solids recovery. In the present test case, a high-efficiency cyclone (pressure drop of 5000 Pa, inlet velocity of 32 m/s, diameter of 1.15 m, height of 1.8 m, vortex finder diameter of 0.36 m) was chosen. As shown in Figure 13, this cyclone is indeed able to decrease the Sauter diameter from 83 to about 73 μm at the end of the 600 h of operation, which is sufficient to decrease the equilibrium bubble size from 7.5 to about 5 cm. The increased mass-transfer area increases the conversion from 68 to 82% (Figure 14). However, the attrition rate in the high-efficiency cyclone is a factor of 5 higher than in the case of the standard cyclone. It should be noted here that the inlet velocity of 32 m/s

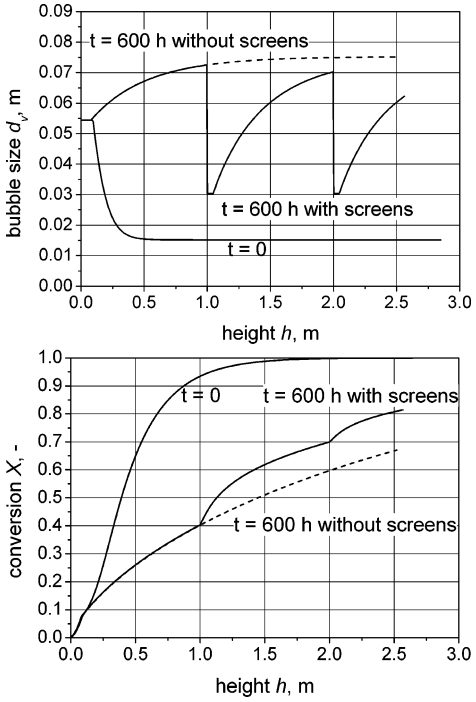

Figure 12. Test case B: Screens for the reduction of bubble sizes (single cyclone of test case A).

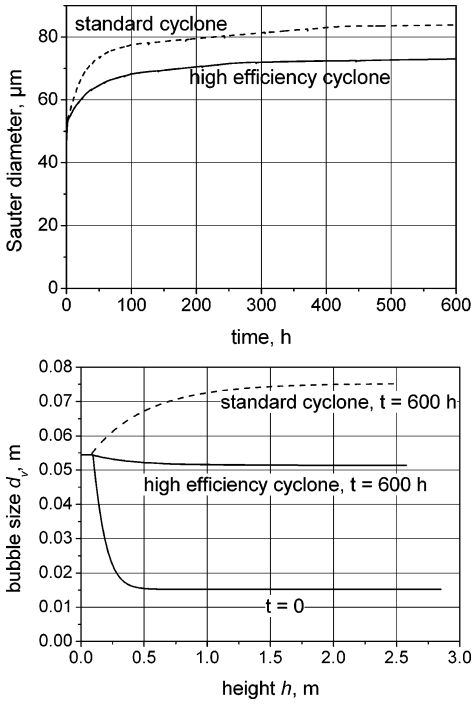

Figure 13. Test case C: one single high-efficiency cyclone.

exceeds the limit of applicability of eq 31,[25] which means that, because of additionally occurring fragmentation, the attrition rate will be even higher than predicted here.

3.5. Test Case D: Solids Recovery with Five Cyclones in Parallel. It is well-known that the efficiency of cyclone separation increases with decreasing size of the cyclone. In test case D, the standard cyclone was therefore replaced by five cyclones of equal size arranged in parallel (pressure drop of 1660 Pa, inlet velocity of 18 m/s, diameter of 0.7 m, height of 1.1 m, vortex finder diameter of 0.22 m). As is obvious from Figure 15, this arrangement does essentially the same

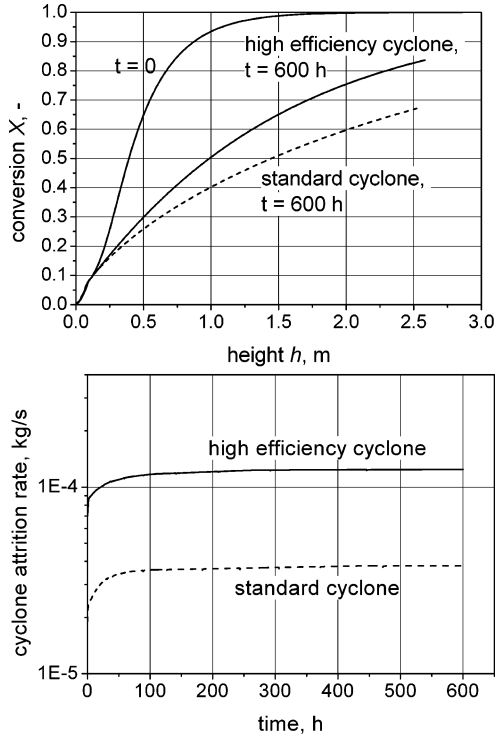

Figure 14. Chemical conversion and cyclone attrition for test case C.

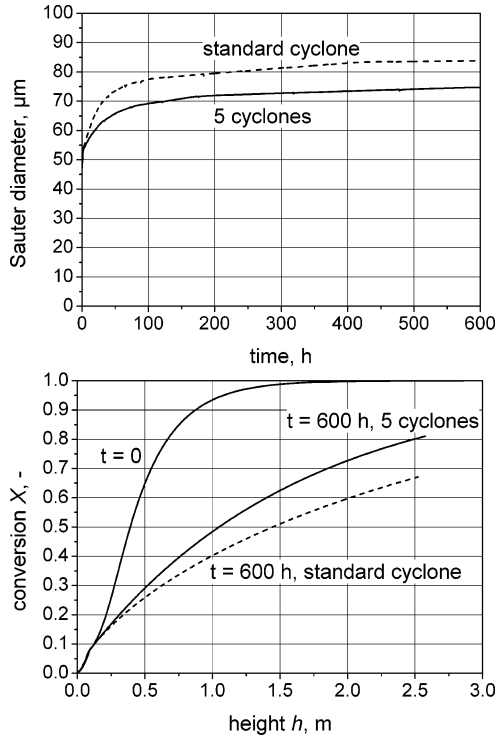

Figure 15. Test case D: Solids recovery with five cyclones in parallel.

job as the single high-efficiency cyclone but avoids the high pressure drop and the high attrition rate of the latter.

3.6. Test Case E: Solids Recovery by Multistage Cyclone Arrangements. A better solids recovery can certainly be achieved with multistage cyclone arrangements. In a first step, the standard cyclone of test case A was taken as the first stage, followed by a second-stage cyclone characterized by a pressure drop of 3800

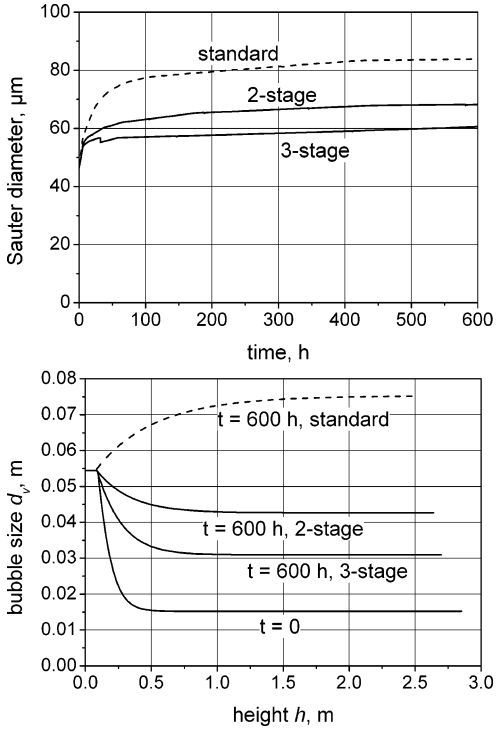

Figure 16. Test case E: Solids recovery by multistage cyclone separation.

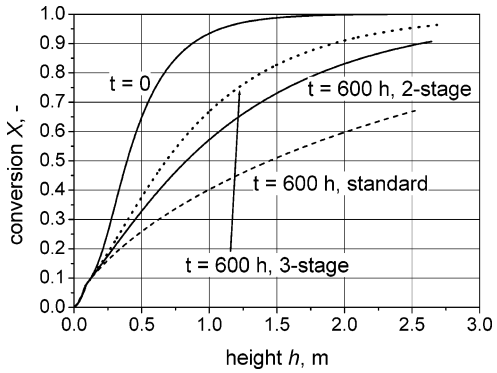

Figure 17. Axial profiles of chemical conversion for multistage cyclone separation.

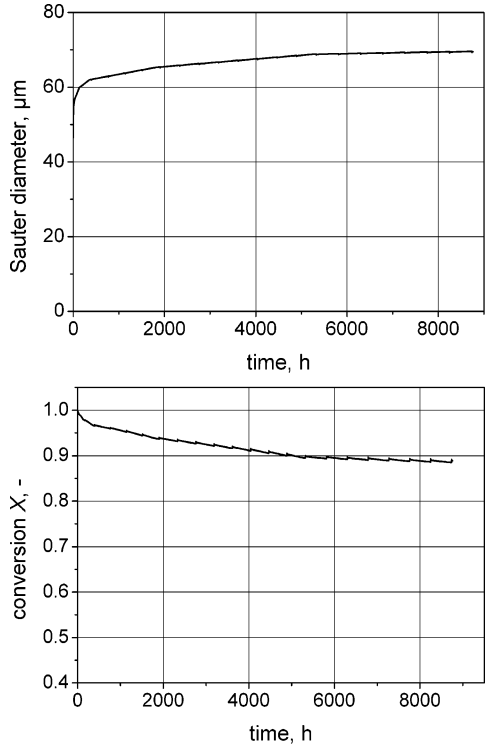

Figure 18. Long-term run for three-stage solids separation.

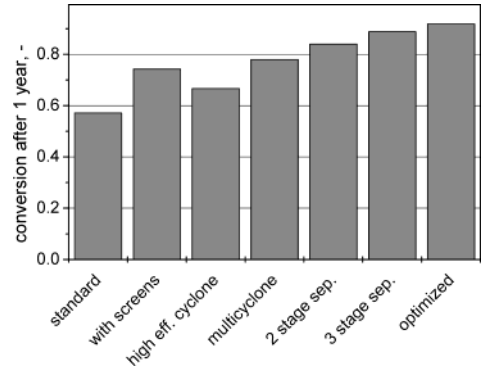

Figure 19. Long-term chemical performances of different reactor configurations.

Pa and an inlet velocity of 25 m/s (as well as a diameter of 1.35 m, a height of 2.1 m, a vortex finder diameter of 0.42 m). In a second step, this arrangement was modified to a three-stage separation by simply adding another cyclone with the same design as the secondary cyclone as the third separation stage. The results of the simulation runs are shown in Figures 16 and 17. We see that, with increasing overall efficiency of the solids recovery, the Sauter diameter in the system is kept at a lower level, which then decreases the equilibrium bubble size (and this increases the mass-transfer area in the bed). As a consequence, the conversion is increased. In the end, the three-stage separation leads to a conversion of over 95%, which is close to that obtained with the fresh catalyst (Figure 17).

For the three-stage separation case, the reactor performance was calculated over a time of operation of 8760 h. Figure 18 shows the result. Although it appears as if the Sauter diameter stabilizes after 5000 h of operation, the conversion seems to decrease further. Obviously, the attrition process that ultimately grinds each particle, irrespective of its initial size, down to an elutriable size takes a very long time to reach a quasi-steady state for the particle population in a fluidized-bed system.

3.7. Comparison of Different Reactor Configurations. Figure 19 compares the long-term chemical performances of the different reactor configurations investigated. The "standard" configuration is the one single cyclone of test case A. We see that the introduction of screens increases the conversion from below 60% to above 70%. The single high-efficiency cyclone is not as good, but the "multicyclone" arrangement with its five cyclones in parallel is even better than the screen solution. The multistage solids recovery systems exhibit the best performance. The "optimized" arrangement means a three-stage separation with the single standard cyclone in the first stage replaced by the five cyclones in parallel. In each case, the decisive parameter for the chemical performance is the Sauter diameter of the bed particles. Figure 20 correlates the Sauter diameters of the different configurations with the chemical conversion for an operating time of 1 year: the more efficient the solids recovery, the better the chemical conversion. The same effect has been observed by Pell and Jordan,[31] who investigated the synthesis of acrylonitrile from

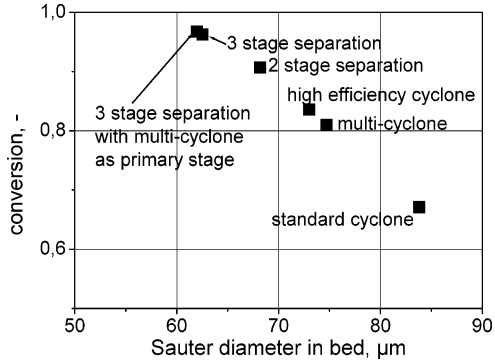

Figure 20. Influence of the Sauter diameter of the bed particles on the chemical conversion.

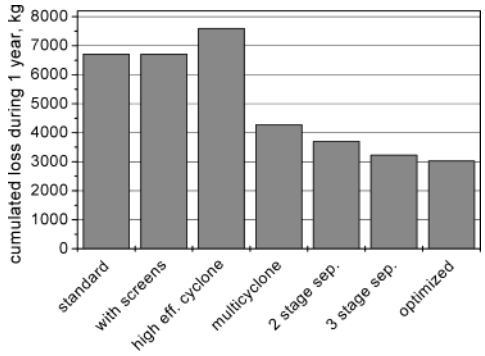

Figure 21. Catalyst losses with different reactor configurations.

propylene and by de Vries et al.[6] in the 3-m-diameter reactor of the Shell Chlorine Process. The plot of Figure 20 should, however, not lead to the conclusion that the conversion is directly related to the mean catalyst particle size or to the outer particle surface area. In reality, there is a long chain of mechanisms leading from the Sauter diameter of the bed particles to the chemical conversion of the reactor: A change of the Sauter diameter varies the minimum fluidization velocity, u_{mf}, first, which via the parameter λ (eq 14) influences bubble splitting and hence the bubble size, which is finally reached as a result of the competition between bubble coalescence and splitting (eq 13). The resulting bubble size determines the local mass-transfer area a (eq 29) between the bubbles and the surrounding suspension phase, and this finally influences the chemical conversion, following eqs 26 and 27.

A major factor for the profitability of a catalytic fluid-bed process is often the cost of the catalyst. Figure 21 compares the cumulative losses of catalyst mass during 1 year of operation. We see that the more sophisticated solids recovery systems manage to halve the catalyst losses compared to the simpler configuration. It should be noted here that the attrition action of the baffles on the catalyst particles has not been considered in the present calculation.

Depending on the reaction and on the catalyst properties, the catalyst might age to such an extent that a periodic renewal of the catalyst in the system becomes necessary. How would this influence the present calculations? In Figure 22, the conversion is plotted against operating time for the conditions of test case A. The simulation was carried out once without and once with catalyst renewal. The renewal was carried out such that, after each week, 1% of the bed inventory was exchanged by fresh catalyst. The simulation yields practically no difference between the two modes of operation. In

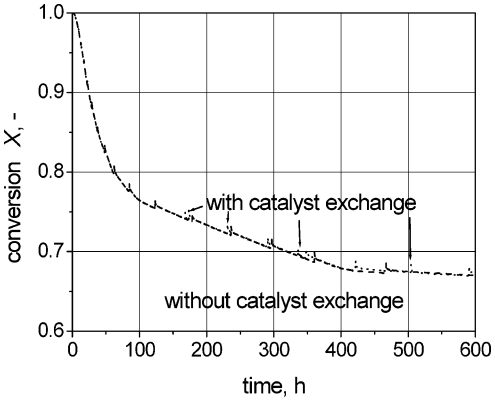

Figure 22. Time-dependent conversion with and without weekly exchange of aged catalyst by fresh catalyst.

addition to the spikes that indicate the replacement of lost catalyst, we see similar spikes after the addition of fresh catalyst. The behavior of the system is thus not influenced as long as the amount of exchanged material and the frequency of exchange are low.

4. Conclusions

In cases where fine particles of the Geldart A type are involved and mass transfer between the bubbles and the suspension phase is limiting, the modeling of industrial fluidized-bed reactors requires a careful consideration of the influence of the bed particle size distribution on the conversion.

The bed particle size distribution develops under the combined influences of catalyst attrition and efficiency of solids recovery. The model simulations reveal that it might take months until an equilibrium particle size distribution has been established and the reactor has reached a quasi-steady state of operation.

The fluidized-bed reactor model presented here takes proper account of the relevant effects and might therefore be helpful for the solution of practical problems in industry.

Acknowledgment

The authors would like to thank the Deutsche Forschungsgesellschaft for financial support under grant WE 935-4.

Nomenclature

a = specific interfacial area, m^2/m^3
A_t = cross-sectional area of reactor, m^2
c_b, c_c, c_j = attrition rate constants, defined by eqs 24, 31, and 23, respectively
c_v = solids volume concentration
C_b, C_d = reactant concentrations in bubble and dense phases, respectively, mol/m^3
C_0 = reactant inlet concentration, mol/m^3
d_{or} = orifice diameter, m
d_p = particle diameter, m
d_v = bubble volume-equivalent sphere diameter, m
$d_{v,0}$ = initial bubble size, from eq 12
d_t = reactor diameter, m
D = diffusion coefficient, m^2/s
g = acceleration due to gravity, m/s^2
$G_{s,\infty}$ = entrainment rate above TDH, $kg/(m^2 \cdot s)$
h = height above gas distributor, m
H_b = height of bed surface above distributor, m
H_j = height of jet region, m

k_G = mass-transfer coefficient, m/s
K_i^* = elutriation rate constant, defined by eq 21
k_m = reaction rate constant, $m^3/(kg \cdot s)$
L = jet length, m
m = mass, kg
$m_{att,i}$ = attrited mass in the size interval i, kg
$\dot{m}_{c,in}$ = solids mass flow at cyclone inlet, kg/s
n_{or} = number of orifices in the gas distributor
N_p = number of particles
$Q_3(d_p)$ = cumulative mass distribution of particle sizes
t = time, s
u = superficial fluidizing velocity, m/s
u_{mf} = minimum fluidizing velocity (superficial), m/s
$u_{c,in}$ = velocity in cyclone inlet, m/s
u_{or} = exit velocity at distributor opening, m/s
u_t = terminal velocity of a single particle, m/s
$\dot{V}_{or}$ = volumetric flow through distributor opening, m/s
$\dot{V}_b$ = visible bubble flow, $m^3/(m^2 \cdot s)$
x = mass fraction

Greek Letters

α = opening half-angle of gas jet, °
ϑ = parameter defined by eq 17
ϵ_b = local bubble volume fraction
ϵ_p = voidage of bed particles
ϵ_{mf} = bed voidage at minimum fluidization conditions
λ = mean duration of life of a bubble, eq 14, s
ς_s = apparent density of bed particles, kg/m^3
ς_g = gas density, kg/m^3
μ_c = ratio of solids mass flow to gas mass flow at cyclone inlet

Literature Cited

(1) Kunii, D.; Levenspiel, O. *Fluidization Engineering*; Butterworth-Heinemann: Boston, 1991.

(2) Squires, A. M. Contributions Toward a History of Fluidization. In *CIESC/AIChE Proceedings of the Joint Meeting on Chemical Engineering*; Chemical Engineering Press: Beijing, 1982; Vol. I, pp 322−353.

(3) May, W. G. Fluidized-Bed Reactor Studies. *Chem. Eng. Prog.* **1959**, *55*, 49.

(4) van Deemter, J. J. Mixing and Contacting in Gas−Solid Fluidized Beds. *Chem. Eng. Sci.* **1961**, *13*, 143.

(5) de Groot, J. H. Scaling-up of Gas-Fluidized Bed Reactors. In *Proceedings of the International Symposium on Fluidization*; Drinkenburg, A. A. H., Ed.; Netherlands University Press: Amsterdam, Netherlands, 1967; p 348.

(6) de Vries, R. J.; van Swaaij, W. P. M.; Mantovani, C.; Heijkoop, A. Design Criteria and Performance of the Commercial Reactor for the Shell Chlorine Process. In *Proceedings of the 5th European Symposium on Chemical Reaction Engineering*; Elsevier Publ. Corp.: Amsterdam, Netherlands, 1972; Vol. 9, p 59.

(7) Gidaspow, D. *Multiphase Flow and Fluidization*; Academic Press: Boston, 1994.

(8) Li, J.; Kuipers, J. A. M. Gas−Particle Interactions in Dense Gas-Fluidized Beds. *Chem. Eng. Sci.* **2003**, *58*, 711.

(9) Werther, J.; Reppenhagen, J. Attrition in Fluidized Beds and Pneumatic Conveying Lines. In *Fluidization, Solids Handling and Processing*; Yang, W. C., Ed.; Noyes Publications: Westwood, NJ, 1999; pp 435−491.

(10) Davidson, J. F.; Harrison, D. *Fluidised Particles*; Cambridge University Press: Cambridge, U.K., 1963.

(11) Merry, J. M. D. Penetration of Vertical Jets into Fluidized Beds. *AIChE J.* **1975**, *3*, 507.

(12) Clift, R.; Grace, J. R. Bubble Interaction in Fluidized Beds. *Chem. Eng. Prog. Symp. Ser.* **1970**, *66*, 14.

(13) Clift, R.; Grace, J. R. Bubble Coalescence in Fluidized Beds: Comparison of Two Theories. *AIChE Symp. Ser.* **1971**, *67*, 23.

(14) Werther, J. Bubble Growth in Large Diameter Fluidized Beds. In *Fluidization Technology*; Keairns, D. L., Ed.; Hemisphere Publishing: Washington, DC, 1976; Vol. I, pp 215−235.

(15) Hilligardt, K.; Werther, J. The Influence of Temperature and Solids Properties on the Size and Growth of Bubbles in Gas Fluidized Beds. *Chem. Eng. Technol.* **1987**, *10*, 272.

(16) Tasirin, S. M.; Geldart, D. Entrainment of FCC from Fluidized Beds−A New Correlation for the Elutriation Rate Constants. *Powder Technol.* **1998**, *95*, 240.

(17) Werther, J.; Xi, W. Jet Attrition of Catalyst in Gas Fluidized Beds. *Powder Technol.* **1993**, *76*, 39.

(18) Xi, W. Katalysatorabrieb in Wirbelschichtreaktoren. Ph.D. Dissertation, Technical University Hamburg-Harburg, Hamburg, Germany, 1993.

(19) Werther, J.; Reppenhagen, J. Catalyst Attrition in Fluidized-Bed Systems. *AIChE J.* **1999**, *45*, 2001.

(20) Sit, S. P.; Grace, J. R. Effect of Bubble Interaction on Interphase Mass Transfer in Gas Fluidized Beds. *Chem. Eng. Sci.* **1981**, *36*, 327.

(21) Basov, V. A.; Markhevka, V. I.; Melik-Akhnazarov, T. Kh.; Orochko, V. Investigation of the Structure of a Nonuniform Fluidized Bed. *Int. Chem. Eng.* **1969**, *9*, 263.

(22) Sitzmann, W.; Werther, J.; Böck, W.; Emig, G. Modelling of Fluidized Bed Reactors−Determination of Suitable Kinetics for Complex Reactions. *Ger. Chem. Eng.* **1985**, *8*, 301.

(23) *VDI Heat Atlas*; VDI Verlag: Duesseldorf, Germany, 1997.

(24) Trefz, M.; Muschelknautz, E. Extended Cyclone Theory for Gas Flows with High Solids Concentrations. *Chem. Eng. Technol.* **1993**, *16*, 153.

(25) Reppenhagen, J.; Werther, J. Catalyst Attrition in Cyclones. *Powder Technol.* **2000**, *11*, 55.

(26) Reppenhagen, J.; Werther, J. The Role of Catalyst Attrition in the Adjustment of the Steady-State Particle Size Distribution in Fluidized Bed Systems. In *Fluidization X*; Kwauk, M., Li, J., Yang, W. C., Eds.; Engineering Foundation: New York, 2001; p 69.

(27) Matsen, J. M. Evidence of Maximum Stable Bubble Size in a Fluidized Bed. *AIChE Symp. Ser.* **1973**, *69*, 30.

(28) Pell, M. *Gas Fluidization*; *Handbook of Powder Technology*; Elsevier: Amsterdam, 1990; Vol. 8.

(29) Grace, J. R.; Sun, G. Influence of Particle Size Distribution on the Performance of Fluidized Bed Reactors. *Can. J. Chem. Eng.* **1991**, *69*, 1126.

(30) Bauer, W.; Werther, J. Modeling Complex Reaction Systems in Fluidized-Bed Reactors. *ACS Symp. Ser.* **1982**, *196*, 121.

(31) Pell, M.; Jordan, S. P. Effects of Fines and Velocity on Fluid Bed Reactor Performance. *AIChE Symp. Ser.* **1988**, *84*, 68.

(32) Bauer, W.; Werther, J.; Emig, G. Influence of Gas Distributor Design on the Performance of Fluidized Bed Reactors. *Ger. Chem. Eng.* **1981**, *4*, 291.

(33) Werther, J. Scale-up Modeling for Fluidized Bed Reactors. *Chem. Eng. Sci.* **1992**, *47*, 2457.

Received for review October 13, 2003
Revised manuscript received March 1, 2004
Accepted March 2, 2004

IE030760T